may have been highly conserved throughout evolution.

References and Notes

1. S. D. Bell, S. P. Jackson, *Curr. Opin. Microbiol.* **4**, 208 (2001).
2. M. Grunstein, *Nature* **389**, 349 (1997).
3. L. Guarente, *Genes Dev.* **14**, 1021 (2000).
4. D. Moazed, *Mol. Cell.* **8**, 489 (2001).
5. R. A. Frye, *Biochem. Biophys. Res. Commun.* **273**, 793 (2000).
6. J. Min, J. Landry, R. Stemglanz, R.-M. Xu, *Cell* **105**, 269 (2001).
7. Q. She *et al.*, *Proc. Natl. Acad. Sci. U.S.A.* **98**, 7835 (2001).
8. Supplementary material is available on *Science* Online at www.sciencemag.org/cgi/content/full/296/5565/148/DC1.
9. J. C. Tanny, D. Moazed, *Proc. Natl. Acad. Sci. U.S.A.* **98**, 415 (2001).
10. J. C. Tanny, G. J. Dowd, J. Huang, H. Hilz, D. Moazed, *Cell* **99**, 735 (1999).
11. P. Forterre, F. Confalonieri, S. Knapp, *Mol. Microbiol.* **32**, 669 (1999)
12. S. D. Bell, S. S. Cairns, R. L. Robson, S. P. Jackson, *Mol. Cell* **4**, 971. (1999).
13. C. P. Magill, S. P. Jackson, S. D. Bell, *J. Biol. Chem.* **276**, 46693 (2001)

14. This work was funded by the Medical Research Council, BBSRC and Cancer Research Campaign. M.F.W. is a Royal Society University Research Fellow. We thank L. Ko Ferrigno for help preparing this manuscript.

4 February 2002; accepted 27 February 2002

Crystal Structure of the Extracellular Segment of Integrin αVβ3 in Complex with an Arg-Gly-Asp Ligand

Jian-Ping Xiong,[1] Thilo Stehle,[1,2*] Rongguang Zhang,[3*] Andrzej Joachimiak,[3] Matthias Frech,[4] Simon L. Goodman,[5] M. Amin Arnaout[1†]

The structural basis for the divalent cation–dependent binding of heterodimeric αβ integrins to their ligands, which contain the prototypical Arg-Gly-Asp sequence, is unknown. Interaction with ligands triggers tertiary and quaternary structural rearrangements in integrins that are needed for cell signaling. Here we report the crystal structure of the extracellular segment of integrin αVβ3 in complex with a cyclic peptide presenting the Arg-Gly-Asp sequence. The ligand binds at the major interface between the αV and β3 subunits and makes extensive contacts with both. Both tertiary and quaternary changes are observed in the presence of ligand. The tertiary rearrangements take place in βA, the ligand-binding domain of β3; in the complex, βA acquires two cations, one of which contacts the ligand Asp directly and the other stabilizes the ligand-binding surface. Ligand binding induces small changes in the orientation of αV relative to β3.

Integrins are adhesion receptors that mediate vital bidirectional signals during morphogenesis, tissue remodeling, and repair [reviewed in (*1*)]. These heterodimers are formed by the noncovalent association of an α and a β subunit, both type I membrane proteins with large extracellular segments. In mammals, 18 α and 8 β subunits assemble into 24 different receptors. Integrins depend on divalent cations to bind their extracellular ligands. Although these ligands are structurally diverse, they all use an acidic residue during integrin recognition. Specificity for a particular ligand is then determined by additional contacts with the integrin. High affinity binding of integrins to ligands is usually not constitutive but is elicited in response to cell "activation" signals (so-called "inside-out" signaling) that alter the tertiary and quaternary structure of the extracellular region, making the integrin ligand-competent. Ligand binding, in turn, induces structural rearrangements in integrins that trigger "outside-in" signaling [reviewed in (*2*)].

Integrins are grouped into two classes based on the presence or absence of an extracellular ~180 amino acid A-type domain (αA) (*3*). In the nine αA-containing integrins (αA-integrins), αA is necessary and sufficient for the divalent cation–dependent binding to physiologic ligands (*3*). The structures of isolated αA domains in "liganded" and "unliganded" conformations (*4–8*) have revealed how this domain interacts with ligands. A metal ion is coordinated at the ligand-binding interface of αA through a conserved five amino acid motif, the metal ion–dependent adhesion site (MIDAS), and the metal coordination is completed by a glutamate from the ligand (*4*, *6*) or, in its absence, by a water molecule (*9*). In αA-lacking integrins, ligand recognition requires an αA-like domain (βA) present in all integrin β subunits (*4*, *10*).

The crystal structure of the extracellular segment of the αA-lacking integrin αVβ3 was previously determined in the presence of Ca^{2+} (αVβ3-Ca) (*10*). It consists of 12 domains assembled into an ovoid head and two "legs." The putative ligand-binding head is primarily formed of a seven-bladed β-propeller domain from αV and a βA domain from β3. These two domains resemble the Gβ and Gα subunits of G-proteins, respectively, and contact each other in a strikingly similar manner (*10*). We now report the structure of extracellular αVβ3 in complex with the cyclic pentapeptide ligand Arg-Gly-Asp-{D-Phe}-{*N-methyl*-Val-}, called cyclo(RGDF=N{Me}V [P5 in (*11*)], and in the presence of the proadhesive cation Mn^{2+}, αVβ3-RGD-Mn (Table 1). We have also determined the structure of the unliganded receptor in the presence of Mn^{2+} (αVβ3-Mn) for comparison (Table 1). The two structures contain the previously reported extracellular residues of the integrin (*10*). αVβ3-Mn contains six Mn^{2+} ions (replacing each of the six Ca^{2+} ions in αVβ3-Ca), and αVβ3-RGD-Mn contains the cyclic pentapeptide plus eight Mn^{2+} ions. Replacement of Ca^{2+} with Mn^{2+} at all six sites in the αVβ3-Mn structure did not result in important structural rearrangements in the integrin. As with αVβ3-Ca (*10*), no metal ion is visible at MIDAS in αVβ3-Mn. Figure 1 shows representative electron density maps (Fig. 1, A through D) and a ribbon diagram (Fig. 1E) of the integrin-pentapeptide complex.

The αVβ3-RGD-Mn structure reveals that the pentagonal peptide inserts into a crevice between the propeller and βA domains on the integrin head (Fig. 1E). The Arg-Gly-Asp, or RGD, sequence makes the main contact area with the integrin, and each residue participates extensively in the interaction, which buries 355 Å^2 or 45% of the total surface area of the peptide. The Arg and Asp side chains point in opposite directions, exclusively contacting the propeller and βA domains, respectively. The five Cα atoms of the cyclic peptide form a slightly distorted pentagon. Molecular dynamics simulations of the peptide in the absence of the integrin, performed using the same geomet-

[1]Renal Unit, Leukocyte Biology and Inflammation Program, Structural Biology Program, Massachusetts General Hospital, 149 13th Street, Charlestown, MA 02129, USA. [2]Laboratory of Developmental Immunology, Massachusetts General Hospital, and Harvard Medical School, 55 Fruit Street, Boston, MA 02114, USA. [3]Argonne National Laboratory, Biosciences Division, Structural Biology Center, IL 60439, USA. [4]Department of Target Research, [5]Biomedical Research, Oncology, Merck KGaA, Darmstadt 64271, Germany.

*These two authors contributed equally to this work. †To whom correspondence should be addressed. E-mail: arnaout@receptor.mgh.harvard.edu

ric parameters used for the crystallographic refinement, result in a more regular pentagonal shape with roughly equal inter–Cα atom distances (data not shown). Thus, distortion of the peptide ring is apparently related to contact with αVβ3-Mn. The main chain conformation of the RGD motif in the pentapeptide is almost identical to that of the RGD tripeptide in the natural ligand Echistatin (*12*, *13*), suggesting that the structure presented here can serve as a basis for understanding the interaction of integrins with other and larger RGD-containing ligands.

The Arg side chain inserts into a narrow groove at the top of the propeller domain (Fig. 2A), formed primarily by the D3-A3 and D4-A4 loops. The arginine guanidinium group is held in place by a bidentate salt bridge to Asp^{218} at the bottom of the groove and by an additional salt bridge to Asp^{150} at the rear (Fig. 2B). The contacts leave most of the upper portion of the Arg side chain exposed to solvent, whereas the spacious rear of the groove probably contains water molecules that may provide additional contacts to the Arg guanidinium group.

Contacts between the ligand Asp and βA primarily involve the Asp carboxylate group, which protrudes into a cleft between the βA loops A′-α1 and C′-α3 and forms the center of an extensive network of polar interactions (Fig. 2B). One of the Asp carboxylate oxygens contacts a Mn^{2+} ion at MIDAS in βA (Fig. 2B). The second Asp carboxyl oxygen forms hydrogen bonds with the backbone amides of Tyr^{122} and Asn^{215} and also contacts the aliphatic portion of the Arg^{214} side chain. Additional contacts involve the hydrophobic portion of the Asp side chain and the beta carbon atom of Asn^{215}. Unlike the ligand Arg, the ligand Asp side chain is completely buried in the complex.

The glycine residue, which completes the prototype RGD ligand sequence, lies at the interface between the α and β subunits (Fig. 2B). It makes several hydrophobic interactions with αV, the most critical of which appears to be the contact with the carbonyl oxygen of Arg^{216}. The remaining two residues of the pentapeptide face away from the αβ interface and are not in the consensus ligand sequence.

The peptidyl aspartate contacts βA in a manner that strikingly resembles the interaction of αA with its ligands (*4*, *6*) (Fig. 3); in both cases, an acidic ligand residue coordinates the receptor via a metal ion in MIDAS. However, βA differs from αA in that the latter can bind a metal ion in MIDAS even in its unliganded state (*5*, *9*). The one difference between the two sites is the replacement of a conserved Thr, which contacts the cation in liganded αA, with Glu^{220} in βA. In the unliganded αVβ3-Mn structure, the Glu^{220} side chain intrudes into the MIDAS site, approaching the space where a cation would bind. Thus, it appears to reduce the affinity for cations at MIDAS through steric hindrance. In the liganded αVβ3-RGD-Mn structure, the Glu^{220} side chain occupies a different position, allowing accommodation of a cation at MIDAS.

In addition to incorporating Mn^{2+} at MIDAS when liganded, βA also unexpectedly incorporates a second Mn^{2+} ion. Only 6 Å from MIDAS, this ion defines a ligand-associated metal binding site (LIMBS) formed by the other carboxylate oxygen of Glu^{220}; the side chains of Asp^{158}, Asn^{215}, and Asp^{217}; and the carbonyl oxygens of Asp^{217} and Pro^{219} (Fig. 2B). Although the LIMBS Mn^{2+} ion does not contact the ligand, coordination of Mn^{2+} nevertheless depends on it. Asp^{158} and Glu^{220} occupy different positions in the unliganded structure, and, therefore, the coordination sphere for LIMBS does not exist. The most likely role of LIMBS is to stabilize the reoriented Glu^{220} and to add conformational stability and structural rigidity to the ligand-binding surface. Taken together, the above data explain the structural basis for conservation of the RGD consensus in integrin ligands and for certain loss-of-function disease mutations in β3 integrins [Supplemental note 2 (*21*)].

Binding of the pentapeptide ligand is associated with tertiary and quaternary changes in αVβ3-Mn. Changes in tertiary structure involve βA, affecting primarily its α1-α2 loops and helices and the α2-C′, F-α7, and B-C ("ligand-specificity") loops (Fig. 4, A and B). The observed movements appear to be causally linked to the top of helix α1 which approaches MIDAS, permitting contacts with both MIDAS cation and ligand through Ser^{121}, Tyr^{122}, and Ser^{123}. In the complex, the backbone amide and carbonyl oxygens of Tyr^{122} directly contact the

Table 1. Data collection and refinement statistics [Supplemental note 1, (*14*)]. Diffraction data were sharpened with a B factor of $-40.0Å^2$. The αVβ3-Mn and αVβ3-RGD-Mn structures were solved by molecular replacement at 3.3 Å and 3.2 Å resolution, respectively, using the previously reported αVβ3-Ca structure as the initial model. For the αVβ3-Mn structure, the original coordinates were modified by removing all six calcium ions. Coordinates were then subjected to rigid body minimization. A $F_o - F_c$ difference map showed positive density in all six previously determined calcium-binding sites. The eight metal ion densities in the structure were all assigned as manganese because crystals were soaked with buffer containing 5 mM $MnCl_2$. The positions of manganese ions were confirmed from the anomalous difference Fourier maps using data collected at the wavelength 1.2398 Å, where Mn^{2+} has reasonable anomalous contribution (f″ = 1.96 electrons). For the αVβ3-RGD-Mn structure, a similar $F_o - F_c$ difference density map showed clear density for all five amino acids of the cyclic peptide ligand and for eight Mn^{2+} ions: six at the original sites and two in the vicinity of the ligand. Each model was then modified according to the difference density features and refined using bulk solvent correction and several rounds of simulated annealing protocols in XPLOR (*22*). About 5% of reflections were used to calculate the free *R* factor in each case. The reflections included in the two "free sets" were the same as those used for the αVβ3-Ca structure determination. The electron density maps calculated with the three independent data sets (for αVβ3-Ca, αVβ3-Mn, and αVβ3-RGD-Mn) do not allow us to trace the PSI, EGF-1, and EGF-2 domains. In addition, these three density maps show some variability in the NH_2-terminal part of EGF-3, leaving open the possibility that alternative disulphide bridges in this region exist.

	αVβ3-Mn	αVβ3-RGD-Mn
	*Data collection statistics**	
Space group	$P3_221$	$P3_221$
Unit cell dimensions (Å)	a = b = 130.4, c = 310.3	a = b = 129.8, c = 308.8
Resolution (Å)	50.0 to 3.3	50.0 to 3.2
Completeness	94.4 (86.1)	99.4 (99.9)
Unique reflections	44739 (4011)	48911 (4853)
Redundancy	4.8 (3.0)	6.7 (6.0)
R_{sym} (%)†	9.5 (43.9)	16.4 (40.0)
I/σ	16.1 (2.5)	14.0 (3.7)
	Refinement statistics	
Resolution (Å)	20.0 to 3.3	20.0 to 3.2
R_{factor} (%) (work set)‡	24.4	24.8
R_{factor} (%) (free set)	32.3	32.8
Average B factor ($Å^2$)	44.8	36.0
Atoms in the model	11656	11700 (including peptide)
No. Glc-NAc	11	11
No. Mn^{2+}	6	8
	Model statistics (RMSD from ideality)	
Bond lengths (Å)	0.01	0.001
Bond angles (°)	1.7	1.8
Dihedral angles (°)	26.5	26.8

*Values in parentheses are for the highest resolution shell (0.1 Å). †$R_{sym} = \Sigma|I - \langle I\rangle|/\Sigma I$, where *I* is the observed intensity and $\langle I\rangle$ is the average intensity from multiple observations of symmetry-related reflections. ‡$R_{factor} = \Sigma_{hkl} |F_o(hkl) - F_c(hkl)| / \Sigma_{hkl} F_o(hkl)$.

ligand Asp, and both serine side chains coordinate the MIDAS cation. Thus, α1 is fastened to the ligand-MIDAS assembly within the complex. The ADMIDAS (adjacent to MIDAS) cation moves in concert with α1 because it is primarily coordinated by α1 residues Asp^{126} and Asp^{127}; this changes its coordination sphere slightly from that of the unliganded structure (*10*) (only its coordination by the carbonyl oxygen of Met^{335} is replaced by a carboxylate oxygen from Asp^{251}). Most of the remaining structural changes can be viewed as indirectly caused by the shift of α1: α1′ directly follows α1 in sequence, and α2 and the top of α7 flank α1′. The ligand-specificity region also approaches the ligand. This movement may be related to a salt bridge in this region between Asp^{179} and Arg^{214}. Arg^{214} is near the ligand Asp, and it does not form a salt bridge to Asp^{179} in the unliganded structure. The functional implications of these changes are reflected by the location in the α1-α2 segment of βA of epitopes both for activation and inhibitory monoclonal antibodies (*15*–*18*).

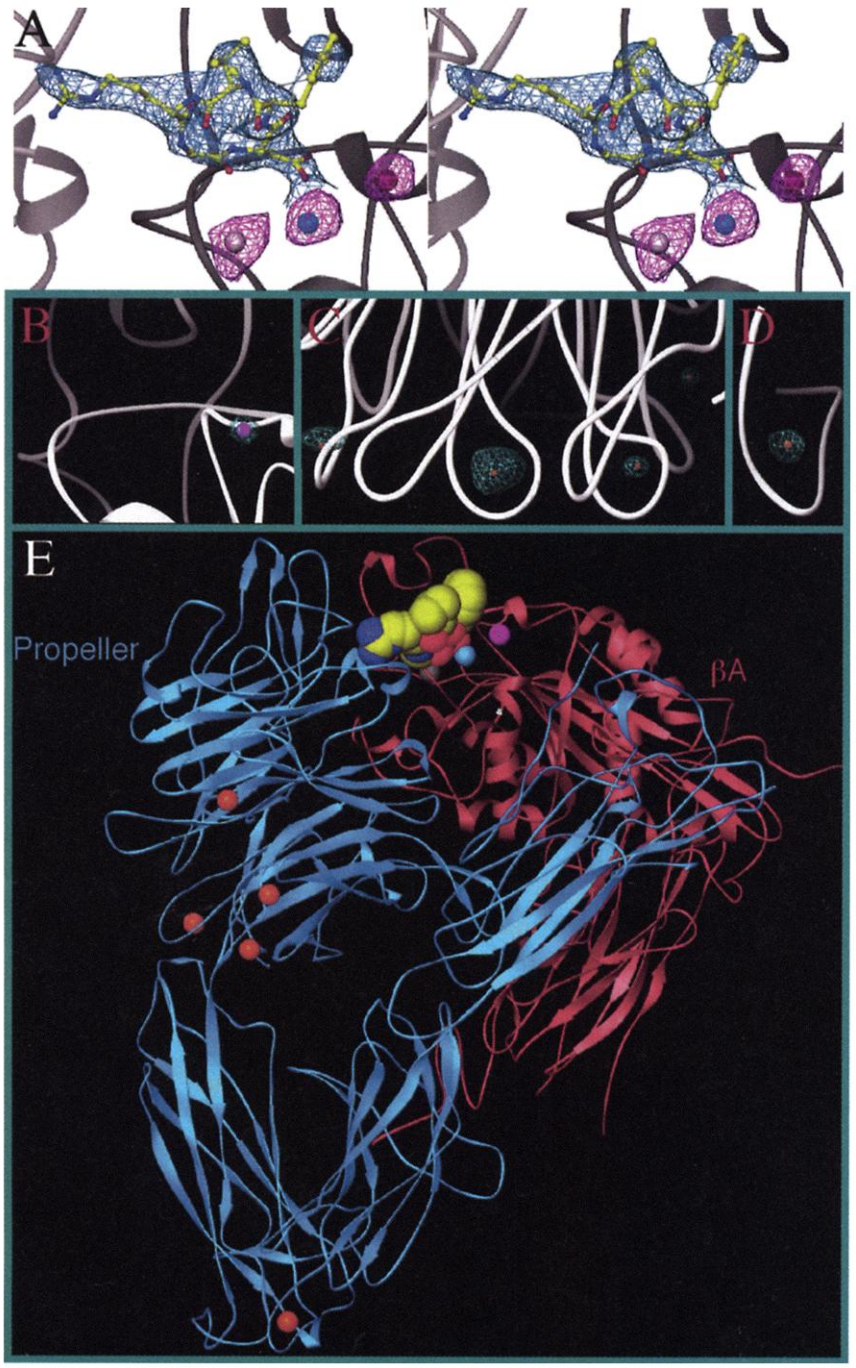

Fig. 1. Structure of αVβ3-Mn complexed with cyclo(RGDf-N{Me}V). (**A**) Stereoview of a $2F_o - F_c$ electron density map of the peptide-integrin complex, where o and c are the observed and calculated structures, respectively. Cutoff is 5.0σ for Mn^{2+} and 1.0σ for ligand residues. Densities (magenta) of the adjacent metal ions at ADMIDAS, MIDAS, and LIMBS (shown here and in subsequent figures as violet, cyan, and gray respectively) are from the same map. (**B**) A Fourier anomalous difference map in the same region as in (A) of αVβ3-Mn; only the density (cyan) of the Mn^{2+} ion at ADMIDAS is detected. (**C** and **D**) A Fourier anomalous difference map showing the densities (cyan) of the Mn^{2+} ions (orange), four in β hairpin loops of blades 4 to 7 of the propeller (C) and one at the αV genu (D) in the peptide-integrin complex. (**E**) Ribbon drawing (*20*) of the αVβ3-RGD-Mn structure. In this and subsequent figures, αV and β3 are shown in blue and red, respectively. The peptide is bound at the propeller-βA domain interface with the ADMIDAS, MIDAS, and LIMBS metal ions shown. The carbon, nitrogen, and oxygen atoms of cyclo(RGDf-N{Me}V) are shown in yellow, blue, and red, respectively.

The above tertiary changes observed in the liganded form of βA resemble those seen in liganded αA (*6*, *8*, *9*) (Fig. 4). In αA, a major distinguishing feature of its transition from the unliganded to the liganded state is a 10 Å downward shift of the COOH-terminal α7 helix with realignment of its hydrophobic contacts (Fig. 4C) (*6*, *8*, *9*). However, the position of the α7 helix in liganded βA does not change (it already occupies an equivalent position to liganded αA when ligand is absent). One likely interpretation of these data is that activation (ligand-competency) in αA and βA is achieved by different mechanisms. Reorientation of the COOH-terminal α7 helix, perhaps in response to inside-out signaling, makes αA ligand-competent in an allosteric manner (*8*). In βA, where such movement of the α7 helix is less likely, reorientation of the MIDAS Glu^{220} residue (which is invariant in βA but not αA domains), results in a ligand-competent form by unblocking MIDAS. A second interpretation of these data is that the conformation of βA in the unliganded αVβ3-Mn and αVβ3-Ca structures represents a ligand-competent state of the A-type domain, captured in the context of an integrin heterodimer. In this scenario, the tertiary changes observed here in βA are ligand-induced.

Quaternary rearrangements in the integrin head region are also observed in the complex. The interface between βA and the αV propeller undergoes a small change, with the two domains moving closer together at the peptide-binding site [see animated Supplemental fig. 1, A and B (*19*)]. In addition, the propeller undergoes a small rotation at the propeller-thigh interface, with βA moving in concert [see animated Supplemental fig. 1, A and B (*19*)]. Thus, as in the case of G-proteins, ligand binding to βA alters its orientation relative to the propeller. It is also remarkable that both tertiary and quaternary changes are observed in an integrin in the presence of its smallest recognition unit, even within the constrained crystal lattice. Natural integrin ligands are significantly larger, structurally diverse and often multivalent. Thus, the

present conformational rearrangements likely represent a minimalist view of the scope of changes in the receptor that take place during integrin-ligand interactions.

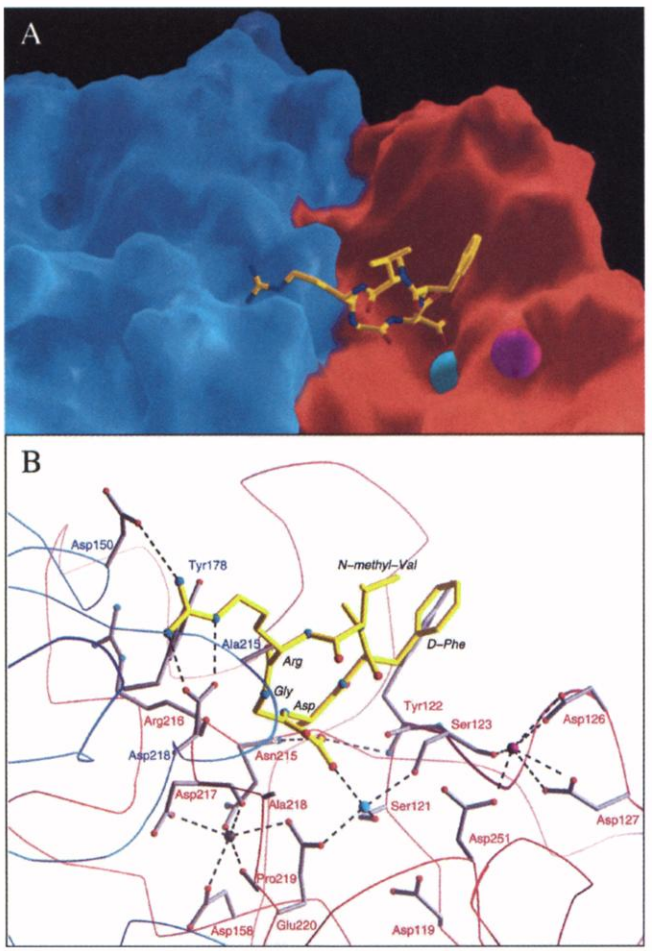

Fig. 2. The ligand-integrin binding site. (**A**) Surface representation of the ligand-binding site, with the ligand peptide shown as ball-and-stick model. Color code for the ligand and the two visible Mn^{2+} ions (MIDAS and ADMIDAS) is as in Fig. 1. (**B**) Interactions between ligand and integrin. The peptide (yellow) and residues interacting with the ligand or with Mn^{2+} ions are shown in ball-and-stick representation. αV and β3 residues are labeled blue and red, respectively. Oxygen and nitrogen atoms are in red and blue, respectively. The three Mn^{2+} ions in β3 at MIDAS, ADMIDAS, and LIMBS are also shown. Hydrogen bonds and salt bridges (distance cutoff, 3.5 Å) are represented with dotted lines.

References and Notes

1. M. J. Humphries, *Biochem. Soc. Trans.* **28**, 311 (2000).
2. E. F. Plow, T. A. Haas, L. Zhang, J. Loftus, J. W. Smith, *J. Biol. Chem.* **275**, 21785 (2000).
3. M. Michishita, V. Videm, M. A. Arnaout, *Cell* **72**, 857 (1993).
4. J.-O. Lee, P. Rieu, M. A. Arnaout, R. Liddington, *Cell* **80**, 631 (1995).
5. A. Qu, D. J. Leahy, *Proc. Natl. Acad. Sci. U.S.A.* **92**, 10277 (1995).
6. J. Emsley, C. G. Knight, R. W. Farndale, M. J. Barnes, R. C. Liddington, *Cell* **100**, 47 (2000).
7. R. Li, P. Rieu, D. L. Griffith, D. Scott, M. A. Arnaout, *J. Cell Biol.* **143**, 1523 (1998).
8. J. P. Xiong, R. Li, M. Essafi, T. Stehle, M. A. Arnaout, *J. Biol. Chem.* **275**, 38762 (2000).
9. J.-O. Lee, L. Anne-Bankston, M. A. Arnaout, R. C. Liddington, *Structure* **3**, 1333 (1995).
10. J. P. Xiong *et al.*, *Science* **294**, 339 (2001).
11. M. A. Dechantsreiter *et al.*, *J. Med. Chem.* **42**, 3033 (1999).
12. R. A. Atkinson, V. Saudek, J. T. Pelton, *Int. J. Pept. Protein Res.* **43**, 563 (1994).
13. V. Saudek, R. A. Atkinson, J. T. Pelton, *Biochemistry* **30**, 7369 (1991).
14. See Supplemental note 1, available on *Science* Online at www.sciencemag.org/cgi/content/full/1069040/DC1.
15. A. Andrieux, M. J. Rabiet, A. Chapel, E. Concord, G. Marguerie, *J. Biol. Chem.* **266**, 14202 (1991).
16. Y. Takada, W. Puzon, *J. Biol. Chem.* **268**, 17597 (1993).
17. A. Mould, A. Garratt, J. Askari, S. Akiyama, M. Humphries, *FEBS Lett.* **363**, 118 (1995).
18. C. Lu, M. Shimaoka, Q. Zang, J. Takagi, T. A. Springer, *Proc Natl Acad Sci U.S.A.* **98**, 2393 (2001).
19. See Supplemental fig. 1, available on *Science* Online at www.sciencemag.org/cgi/content/full/1069040/DC1.
20. M. Carson, *J. Mol. Graph.* **5**, 103 (1987).
21. See Supplemental note 2, available on *Science* Online at www.sciencemag.org/cgi/content/full/1069040/DC1.
22. A. T. Brünger *et al.*, *Acta Crystallogr. D Biol. Crystallogr.* **54**, 905 (1998).

23. We wish to thank A. Jonczyk for providing the pentapeptide ligand and R. Dunker (MerckKGaA) for valuable assistance with protein purification. Supported by grants from the National Institutes of Health (NIDDK, NHLBI, and NIAID) and in part by the U.S. DOE, Office of Biological and Environmental Research (contract W-31-109-Eng-38). The coordinates have been deposited in the Protein Data Bank under the code 1L5G.

14 December 2001; accepted 25 February 2002
Published online 7 March 2002;
10.1126/science.1069040
Include this information when citing this paper.

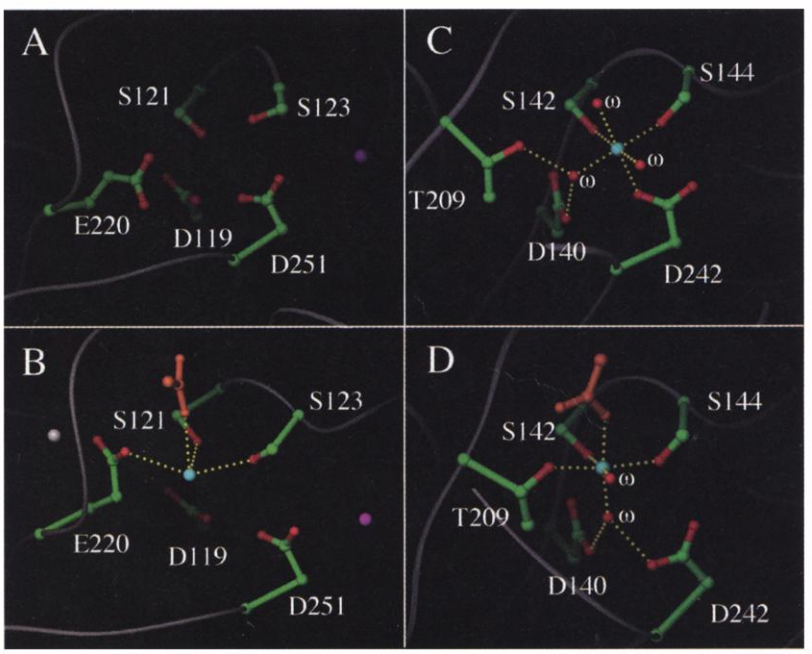

Fig. 3. Diagram of the MIDAS motif in βA (**A** and **B**) and αA from CD11b (**C** and **D**). (A) and (B) MIDAS residues (single letter abbreviations: S, Ser; E, Glu; D, Asp; T, Thr) in unliganded (A) and liganded (B) βA. Coordinating side chains are shown in ball-and-stick representations with oxygen atoms in red, carbon in green; the ligand aspartate is in gold. In addition to the ligand aspartate, the Mn^{2+} (cyan) in the βA MIDAS is coordinated directly with the hydroxyl oxygens of Ser^{121} and Ser^{123} and with one carboxylate oxygen from Glu^{220}. The carboxyl oxygens of Asp^{119} and Asp^{251} of βA lie within 6Å of the metal ion and likely mediate additional contacts through water molecules similar to the liganded forms of αA (D). The Mn^{2+} ion at ADMIDAS (magenta) is present in (A) and (B). The Mn^{2+} ions at MIDAS and at LIMBS (cyan and gray, respectively) are only present in (B). (C) and (D) MIDAS residues in unliganded (C) and liganded (D) αA from CD11b. The metal ion (cyan) is present in both. Water molecules are labeled ω; the pseudoligand glutamate is in gold. Hydrogen bonds and metal ion coordination are represented with dotted yellow lines.

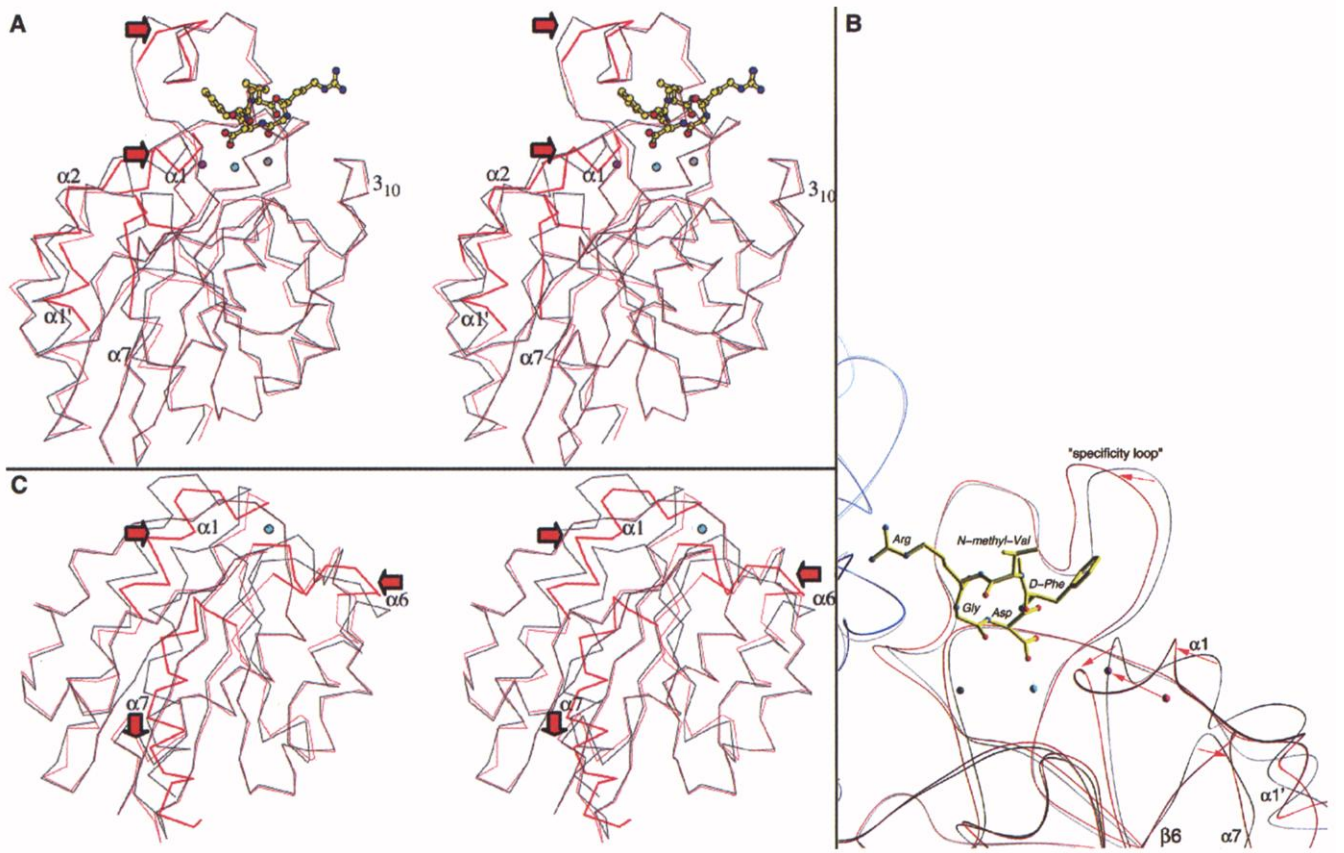

Fig. 4. Ligand-induced structural changes in βA in comparison with those of αA (from CD11b). (**A**) Superposition, in stereo, of the αVβ3-Mn (gray) and αVβ3-RGD-Mn (red) structures. The superposition is based on the Cα atoms of the central β-sheet [43 atoms per structure; root mean square deviation (RMSD), 0.42 Å]. Residues of αVβ3-RGD-Mn with a distance of more than 1.5 Å to corresponding residues of αVβ3-Mn are shown with thicker red lines. The major structural changes in βA involve helices α1, α1′, α2, the F-α7 loop, and the ligand-specificity region. (**B**) Magnified view of the rearrangements at the ligand-binding site in βA. Superposition of the propeller and βA domains of αVβ3-Mn (gray) and αVβ3-RGD-Mn (αV, blue; β3, red) is based on the Cα atoms of the αV propeller domain. The directions of protein movements (including the 4 Å displacement of Mn^{2+} at ADMIDAS) are indicated by red arrows. This view differs from (A) by a rotation of 180° around a vertical axis. (**C**) Superposition, in stereo, of the "liganded" (red) and "unliganded" forms of αA from the CD11b integrin. The metal ion sphere at MIDAS is in cyan. The superposition is based on the Cα atoms of the central β-sheet (43 atoms; RMSD = 0.43 Å). Residues of liganded αA with a distance of more than 1.5 Å to corresponding residues of unliganded αA are shown with thicker red lines. The major structural changes in αA involve helices α1, α7, the F-α7, and E-α6 loops. Arrows (red) indicate the direction of the major protein movements in each case.

Resolution of Lung Inflammation by CD44

Priit Teder,[1] R. William Vandivier,[2] Dianhua Jiang,[1] Jiurong Liang,[1] Lauren Cohn,[1] Ellen Puré,[3] Peter M. Henson,[2] Paul W. Noble[1]*

Successful repair after tissue injury and inflammation requires resolution of the inflammatory response and removal of extracellular matrix breakdown products. We have examined whether the cell-surface adhesion molecule and hyaluronan receptor CD44 plays a role in resolving lung inflammation. CD44-deficient mice succumb to unremitting inflammation following noninfectious lung injury, characterized by impaired clearance of apoptotic neutrophils, persistent accumulation of hyaluronan fragments at the site of tissue injury, and impaired activation of transforming growth factor–β_1. This phenotype was partially reversed by reconstitution with $CD44^+$ cells, thus demonstrating a critical role for this receptor in resolving lung inflammation.

The pathogenesis of pulmonary fibrosis typically exhibits overlapping phases of inflammation and deposition of matrix. Successful repair of tissue injury requires resolution of the inflammatory phase. Recent evidence has suggested that this is an active process requiring the release of soluble mediators as well as interactions between these mediators and cell-surface matrix binding proteins (*1*, *2*). A paradigm has emerged that, following tissue injury, there is an influx of polymorphonuclear leukocytes (PMNs) that subsequently undergo apoptosis and must be removed from tissues to allow normal repair to occur. However, in vivo evidence for a relation between removal of apoptotic PMNs and matrix fragments and successful repair of injury has not been obtained.

CD44 is a transmembrane adhesion receptor and the major cell-surface receptor for the nonsulfated glycosaminoglycan hyaluronan (HA) (*3*). CD44 plays an important role in the clearance of HA and mediates cell-matrix interactions involved in tumor formation, metastasis and T cell extravasation (*4*–*6*). HA is present in all tissues in a high molecular weight (MW) form in excess of 10^6 daltons (*7*). At sites of inflammation and tissue injury low-MW HA species accumulate and have proinflammatory functions (*8*). We examined the role of CD44 in the resolution of lung